

RSC Advances



This is an *Accepted Manuscript*, which has been through the Royal Society of Chemistry peer review process and has been accepted for publication.

Accepted Manuscripts are published online shortly after acceptance, before technical editing, formatting and proof reading. Using this free service, authors can make their results available to the community, in citable form, before we publish the edited article. This *Accepted Manuscript* will be replaced by the edited, formatted and paginated article as soon as this is available.

You can find more information about *Accepted Manuscripts* in the [Information for Authors](#).

Please note that technical editing may introduce minor changes to the text and/or graphics, which may alter content. The journal's standard [Terms & Conditions](#) and the [Ethical guidelines](#) still apply. In no event shall the Royal Society of Chemistry be held responsible for any errors or omissions in this *Accepted Manuscript* or any consequences arising from the use of any information it contains.

The corrosion inhibition effect of Aryl Pyrazolo Pyridines on Copper in hydrochloric acid system: Computational and Electrochemical studies

Sudheer, M. A. Quraishi*

*Department of Chemistry, Indian Institute of Technology (Banaras Hindu University),
Varanasi -221 005, India*

Tel.: +91-9307025126; fax: +91-542-2368428.

E-mail addresses: maquraishi.apc@itbhu.ac.in; maquraishi@rediffmail.com;

Abstract

The inhibition effect of three aryl pyrazole pyridine derivatives namely: 3-methyl-6-oxo-4,5,6,7-tetrahydro-2*H*-pyrazolo[3,4-*b*]pyridine-5-carbonitrile (APP I), 3-methyl-6-oxo-4-(3-phenoxyphenyl)-4,5,6,7-tetrahydro-2*H*-pyrazolo[3,4-*b*]pyridine-5-carbonitrile (APP II) and 3-methyl-6-oxo-4-(thiophen-2-yl)-4,5,6,7-tetrahydro-2*H*-pyrazolo[3,4-*b*]pyridine-5 carbonitrile (APP III) against the corrosion of copper in 0.5 M HCl solution has been systematically investigated by electrochemical impedance spectroscopy, potentiodynamic polarization measurements and quantum chemical methods. A good correlation between the computed energy gap, ΔE , data and the experimental inhibition efficiencies was found. Potentiodynamic polarization measurement results indicate that all three APPs derivatives are cathodic type inhibitors. Among the studied compounds, APP I exhibited the best inhibition activity 92.3% at 1.59 mmol/L. The scanning electron microscopy (SEM) and energy-dispersive X-ray (EDX) spectroscopy confirmed the presence of inhibitors on the copper surface.

Key words: Copper: Impedance: Potentiodynamic polarization: Density functional theory: Acid inhibition.

Introduction

Copper is one of the most preferred metals which are used in several industries owing to its high electrical and thermal conductivity, malleability, relatively noble properties [1]. In order to prevent the dissolution of copper, during picking and cleaning process, inhibited solutions were used [2, 3]. A perusal of the literature reveals that heterocyclic compounds such as 1,3,4-thiadiazole, tetrazole, benzotriazole, azoles and some eco-friendly corrosion inhibitors have been reported to inhibit the corrosion of copper [4-11].

Now days, various experimental and theoretical techniques have been developed to study the structural properties of inhibitor molecules and their activity toward metal surface, but the quantum chemical calculations based on density function theory (DFT) method have become an attractive theoretical method because it gives exact basic vital parameters [12]. Quantum chemical approach is adequately sufficient to forecast the inhibitor effectiveness.

Recently, versatile biologically active pyrazolo[3,4-*b*]pyridines [13-14], were used as good corrosion inhibitors for mild steel in hydrochloric acid [15]. In the present work we investigated the three selected aryl pyrazolo[3,4-*b*]pyridines (APPs) namely 3-methyl-6-oxo-4,5,6,7-tetrahydro-2*H*-pyrazolo[3,4-*b*]pyridine-5-carbonitrile (APP I), 3-methyl-6-oxo-4-(3-phenoxyphenyl)-4,5,6,7-tetrahydro-2*H*-pyrazolo[3,4-*b*]pyridine-5-carbonitrile (APP II) and 3-methyl-6-oxo-4-(thiophen-2-yl)-4,5,6,7-tetrahydro-2*H*-pyrazolo[3,4-*b*]pyridine-5-carbonitrile (APP III) as corrosion inhibitors for copper in 0.5 M HCl solution. The selections of these compounds are based on the consideration that these compounds contain a better π electron conjugation, aromatic ring and heteroatom enhancing a better coordination and adsorption property and their synthesis is high atom economy. The inhibition studies of above aryl pyrazolo[3,4-*b*]pyridine derivatives were assured by electrochemical impedance, potentiodynamic polarization and computational methods. The SEM and EDX techniques

were also used to examine surface morphology of copper with and without inhibitors in hydrochloric solution.

2. Experimental

2.1 *Electrode and Solutions*

The working electrode, for electrochemical impedance and potentiodynamic polarization studies, was cut from a copper sheet of purity 99.9%. The dimensions of working electrode were $8 \times 1 \times 0.025 \text{ cm}^3$ and only 1 cm^2 area was exposed to the electrolyte, while the remaining area was insulated with epoxy resin. To remove the impurity from the surface the working electrode was mechanically abraded using different 600-1200 grades of silicon carbide (SiC) abrasive papers, than degreased in acetone, and dried at ambient temperature [16]. For each test, a freshly abraded electrode was used. The test solution 0.5 M HCl, which was prepared from 37% hydrochloric acid (Merck) analytical grade chemical and double distilled water.

2.2 *Inhibitors*

The inhibitors synthetic route is given in Figure 1, and their synthesis reported elsewhere [17]. Melting points were recorded on a Toshniwal apparatus and are uncorrected. The purity of compounds was checked on thin layers of silica gel in various non-aqueous solvent systems e.g. benzene: ethyl acetate (9:1), benzene: dichloromethane (8:2). IR spectra (KBr) were recorded on a Shimadzu FT IR-8400s spectrophotometer and ^1H NMR and ^{13}C NMR spectra were recorded on a Bruker DRX-300 instrument at 300 and 75, respectively, in CDCl_3 relative to tetramethylsilane as an internal reference and given in Table 1.

2.3 *Electrochemical measurements*

The impedance measurements carried out by Gamry Potentiostat/Galvanostat electrochemical workstation with a Gamry framework based on ESA400 by using a classical three-electrode cell assembly. In this cell the bare copper specimen was served as working

electrode, a platinum electrode and saturated calomel electrode (SCE) were used as counter and reference electrode, respectively. Impedance measurements were carried out at the open-circuit potential in the frequency range from 100 kHz to 10 mHz, with a signal amplitude perturbation of 10 mV and Nyquist plots were obtained.

Potentiodynamic polarization studies were carried out using the same electrochemical workstation and the cell assembly used for impedance studies. The polarization curves were recorded in the potential range of -250 to +250 mV vs. corrosion potential at a scan rate of 1mV/s. For the each experiment newly prepared electrode as well as the test solution were used. Prior to the impedance and potentiodynamic polarization measurements working electrode was immersed in 0.5 M HCl with and without addition of inhibitor for 2 h for stabilization of open circuit potential (OCP) w.r.t. SCE at the ambient temperature. All electrochemical data were assessed by Echem Analyst version 6.03 software packages.

2.4 Cyclic voltammetric studies

Cyclic voltammetry was carried out for bare copper electrode and inhibitor covered electrode in the test solution. The working electrode was scanned from negative to positive in the potential range of -0.4–0.4 V at a scan rate of 20 mV/s.

2.5 Quantum chemical calculations

Quantum chemical calculations using density functional theory (DFT) at the B3LYP/6-31G++ (d, p) basis set level with the Gaussian 03 package were applied to elucidate the structure activity relationship of all APPs. The geometry of all compounds under investigation was determined by optimizing all geometrical variables without any symmetry constraints. These calculations give values of such as the energies of highest occupied molecular orbital (E_{HOMO}), energy of lowest unoccupied molecular orbital (E_{LUMO}), the energy gap ($E_{\text{LUMO}}-E_{\text{HOMO}}$), ΔE , representing the function of reactivity, Mulliken charge, dipole moment, μ of the inhibitor molecule of interest.

2.6 Surface morphology

The SEM images were recorded to ascertain the interaction of inhibitor molecules with metal surface. The copper specimens of size $2.5 \times 2 \times 0.025$ cm were immersed in 0.5 M HCl in absence and presence of 1.59 mmol/L of APP I for 72h. Thereafter, the copper specimens were taken out, washed with distilled water, degreased with acetone, dried at ambient temperature, and mechanically cut into 1 cm^2 sizes for SEM and EDX investigations. Morphological illustrations were taken through SEM model FEI Quanta 200F microscope at an accelerating voltage of 20 kV at 100 \times magnification.

3. Results and discussion

3.1 Electrochemical studies

3.1.1 Electrochemical impedance spectroscopy (EIS) studies

The Nyquist plots are represented in Figure 2a-c for copper with and without various concentrations of APPs in 0.5 M HCl. The Nyquist plots for copper showed two capacitive loops over the frequency range studied [18]. The experimental impedance data were appraised by fitting the equivalent circuit model shown in Figure 3. This model consists of two time constants in series with the uncompensated resistance R_s . A large part of R_s comes from solution resistance. In the first time constant, R_{ct} describes the charge transfer resistance of copper dissolution, between the metal and OHP (outer Helmholtz plane) to the metal/solution interface, in high frequency region. And Q_{dl} , represents the first constant phase element (CPE), for double layer capacitor on the metal/solution interface. In second time constant, Q_f symbolize the CPE of the surface layer (as in a very thin coating), R_f is the resistance of soluble corrosion products or the ion conducting paths that developed in the surface layer and W is the Warburg element for the semi-infinite (unrestricted) layer thickness diffusion [19].

The impedance of the CPE is described as [20, 21]:

$$Z_{\text{CPE}} = (Q(i\omega)^n)^{-1} \quad (1)$$

where Q is a proportionality factor and frequency independent, i is the imaginary number ($i^2 = -1$), ω is the angular frequency ($\omega = 2\pi f$), and n is a CPE exponent.

Thus the impedance of the first time constant is:

$$Z_1 = \frac{R_{\text{ct}}}{1 + Q_{\text{dl}}(i\omega)^n R_{\text{ct}}} \quad (2)$$

The impedance of the second time constant including semi-infinite diffusion is:

$$Z_2 = \frac{R_f}{1 + R_f Q_f (i\omega)^n + R_f W (i\omega)^{0.5}} \quad (3)$$

and the total impedance for the model is defined as:

$$Z_{\text{total}} = R_s + \frac{R_{\text{ct}}}{1 + Q_{\text{dl}}(i\omega)^n R_{\text{ct}}} + \frac{R_f}{1 + R_f Q_f (i\omega)^n + R_f W (i\omega)^{0.5}} \quad (4)$$

Excellent fit with this model was obtained for all experimental data. As an example, the Nyquist plots for free acid solution and optimum concentration of all inhibitors are presented in Figure 4. The fitting procedure gave the results of inhibition efficiencies and other impedance parameters which are compiled in Table 2. From the Table 2, first (CPE), Q_{dl} , have low values for the inhibited compared to non-inhibited solution is usually explained by the displacement of water molecules from the surface due to adsorption of inhibitor molecules. Moreover, n -values changes from (0.58-0.83) also attributed to adsorption of inhibitor molecules and formation of porous layers [22]. The values of R_{ct} increases when the APPs concentration increases, giving consequently a decrease in the corrosion rate. The inhibition efficiency ($\eta_{\%}$) of the inhibitor was estimated by equating the values of charge transfer resistance in the absence (R_{ct}^0) and presence of inhibitor (R_{ct}^i) as follows:

$$\eta_{\%} = \frac{R_{ct}^i - R_{ct}^0}{R_{ct}^i} \times 100 \quad (5)$$

The order of inhibition efficiency is APP I > APP II > APP III, respectively, and maximum inhibition efficiency is 92.0% for APP I. The second CPE, Q_f , is almost like Warburg impedance suggesting that these pores close and a denser surface layer is formed on the copper surface; act as a resistor by blocking the mass transport [23]. It was confirmed by the higher values of R_f (Table 2) in the presence of inhibitor comparatively blank solution.

Figure 5a-c show Bode-Phase plots also denotes two time constant for the same data pictured in the Nyquist plots. In the Bode plot $\log|Z|$ and phase angle (α) are plotted against $\log f$ shown in three distinctive divisions. At the highest frequencies region ($f = 100$ kHz), $\log|Z|$ vs. $\log f$ can be read from horizontal plateau and phase angle tends to (0°) in this frequency range. This is a behaviour of typical ohmic resistor and counterpart to an uncompensated resistance R_s thus for large values of f , $|Z| \rightarrow R_s$ as $f \rightarrow \infty$ [23]. The second segment at intermediate frequencies, $\log|Z|$ vs. $\log f$ with slope values (S) 0.38–0.53 and the phase angle values for blank solution 0.5 M HCl (-33.0), APP I (-48.58), APP II (-47) and APP III (-52.14) at 1.59 mmol/L are observed. The gradual approach of α towards ideal capacitive value (-90), on addition of APPs, may be associated with the slowing down of the rate of dissolution of copper, suggest the formation of a protective layer [24, 25]. A third segment lies in the low f region a horizontal plateau, where $|Z| \rightarrow R_s + R_{ct} + R_f$ as $f \rightarrow 0$ where $\log|Z|$ almost independent of frequency. These $|Z|$ values for inhibited solution are higher than the uninhibited solution implying the protection of copper. Thus the Bode-Phase plots are corroborating with Nyquist results.

3.1.2 Potentiodynamic polarization measurements

The potentiodynamic polarization curves for copper 0.5 M HCl in the absence and presence of the APPs are illustrated in Figure 6 a-c. The calculated electrochemical

parameters, corrosion potential (E_{Corr}), potential hydrogen evolution starts (E_{H_2}), anodic (b_a) and cathodic (b_c) Tafel slopes, corrosion current density (I_{Corr}), current densities ($I_{\text{E(H}_2)}$) at hydrogen evolution potentials and the inhibition efficiency ($\eta\%$) are calculated and given in Table 3. It is clearly seen from Table 3 that the values of I_{Corr} decreased and the $\eta\%$ increased, in the presence of APPs. This effect significantly increased with increasing the concentrations of APP and attained maximum inhibition 92.3% at 1.59 mmol/L for APP I. The inhibition efficiency was calculated from the equation:

$$\eta\% = \frac{I_{\text{corr}}^0 - I_{\text{corr}}^i}{I_{\text{corr}}^0} \times 100 \quad (6)$$

where, I_{corr}^0 and I_{corr}^i are the corrosion current density in absence and in the presence of inhibitor, respectively. The anodic (β_a) and cathodic (β_c) Tafel slopes are also higher in presence of inhibitor relatively without inhibited solution. Further, the cathodic Tafel slopes changes considerably and there is only a small change in the anodic Tafel slope values for the inhibited system. This suggests that during the process of inhibition the inhibitor predominantly controls the cathodic reaction [26]. A shift in corrosion potential (E_{Corr}) values in negative direction also indicates that APPs preferentially inhibits the cathodic reaction [27]. From these data one can recognize distinctly higher inhibition acquired, among APPs, on concentration 1.59 mmol/L and rank them as follows: APP I > APP II > APP III.

In order to explain the potentiodynamic measurements results various mechanism steps are considered which are extensively discussed in the literature [28]. The anodic curves unambiguous divided into three regions also have been reported in previously [29]. As in Figure 6, for inhibitor-free solution, it is observed the first region: an increase of anodic current, starting from E_{ocp} , with increasing at lower over-potential extended to the potential (-30.77 mV) of the peak current density ($i_{\text{peak}} = 8700 \mu\text{A}$) due to the fast dissolution of Cu(0) into Cu^+ (Eq. (7)). Second region is the peak current density



decreased until a minimum current ($i_{\min} = 2000 \mu\text{A}$) is reached having the potential (-0.066 mV) due to slow oxidation of Cu^+ to Cu^{2+} ; as a result of formation of CuCl , (Eq. 9); because of Cu^+ that reacts faster with Cl^- than Cu^{2+} does. And finally, third region of sudden increase



in current density at more positive potentials leading to a limiting current value (i_{lim}) as a result of CuCl_2^- formation (Eq. (10)) which is responsible for copper corrosion due to its dissolution into the bulk solution and/or its further oxidation to Cu^{2+} (Eq. (12)) [30].



On this ground the anodic curves are characterized by a quasi-Tafelian behavior, i.e. the anodic copper dissolution is not solely activation-controlled, but is under diffusion of both, diffusion of CuCl_2^- from the outer Helmholtz plane and electro-dissolution of copper to the solution bulk [23].

In the evaluation of the cathodic branch of the current potential curves Figure 6, the cathodic current density increases up to ~ -162.4 mV (SCE) due to the oxygen diffusion for inhibitor free solution. After that the current plateaus which are observed between ~ -162.4 mV and ~ -372.1 mV (SCE) which is attributed to the diffusion controlled reduction of dissolved oxygen. In the presence of inhibitor molecules in the 0.5 M HCl, the diffusion limited current density of oxygen decreases and shift the potential more negative direction as it was shown Figure 6a-c and given in Table 3. This trend more pronounced with increasing inhibitor concentration. At the hydrogen gas evolution potential these results suggest that

inhibitors form a protective surface film on metal surface and inhibit the reduction of oxygen [31, 32]. These results indicate that the APPs have a stronger influence on the oxygen reduction than on the Cu oxidation reaction. The cathodic reaction is the four-electron reduction of dissolved O₂ according to the following reaction:



On the whole, it is observed that addition of APPs affects both the anodic and cathodic parts of the curves, but the cathodic reaction is inhibited to a greater extent and named as cathodic type inhibitors.

3.2 Cyclic voltammetric study

The cyclic voltammograms for copper electrode in blank and APP I (1.59 mmol/L) inhibited test solution is shown in Figure 7. It can be observed from the curves there are two anodic current peaks and one cathodic peak in blank solution [33]. The first oxidation peak shows the anodic dissolution of copper occurs by reaction (7). Consequently, the second oxidation peak is related to process Cu⁺ to soluble Cu²⁺ by reaction (12). In reverse sweep, on one hand, the corrosion product of CuCl can be partially reduced as described in reaction (9), as a result the concentration of Cl⁻ at the interface of copper and salt layer increases, which leads to a fast dissolution of copper by reaction (7). On the other hand, the corrosion process would be restrained on a certain extent by the increase in salt layer. Because of the competition of dissolution and precipitation of the film on copper an anodic current hump appears in CV plot on the reverse sweep [34]. The stabilities of bare copper and APP I coated electrode have been examined by cyclic voltammetry. Investigation indicates that the peak current and peak potential of the bare and APP I coated electrode have been remained nearly unchanged after 6 cycles with scan rate of 20mVs⁻¹. Another observed key point is that the presence of APP I cause a decrease in the current density of the first anodic peak. It indicates that APP I can effectively inhibit the Cu⁺ oxidation. Also, the decreases in anodic current of

inhibitors are a result of the decreased chloride ion attack on the copper surface by inhibitor molecule adsorption. The second anodic peaks diminish this indicates that APP I can effectively inhibit the Cu^+ oxidation to soluble Cu^{2+} . On this basis this is confirm that APPs are effective inhibitors for copper.

3.3 Quantum calculation

Quantum chemical calculations are used only to correlate experimentally classified inhibition efficiency from different methods, therefore neutral inhibitor molecules are under investigation. Geometrical optimizations of APP I, APP II, and APP III using DFT/B3LYP/6-31G++ (d, p) basis set [35] are depicted in Figure 8a–c. And the Frontier molecular orbital (FMO) density distributions of three APPs are presented in Figure 9a–c. Quantum chemical parameters obtained from the calculations which are responsible for the inhibition efficiency of inhibitors, such as the energy of highest occupied molecular orbital (E_{HOMO}), energy of lowest unoccupied molecular orbital (E_{LUMO}), the energy gap ($E_{\text{LUMO}}-E_{\text{HOMO}}$), ΔE , Mulliken charge, and dipole moment, μ , are collected in Tables 4. It is clear from Table 4 that the values of E_{HOMO} and the E_{LUMO} changes irregular manner, while the values of $E_{\text{LUMO}}-E_{\text{HOMO}}$ are in good correlation with experimental inhibition efficiencies. According to hard–soft–acid–base (HSAB) principle the bonding tendencies of the inhibitors towards the metal atom follow the general rule, hard acids prefer to co-ordinate to hard bases and soft acids prefer to co-ordinate to soft bases. By the same token metal atoms are acknowledged as soft acids. Hard molecules have a high $E_{\text{LUMO}}-E_{\text{HOMO}}$ gap and soft molecules have a small $E_{\text{LUMO}}-E_{\text{HOMO}}$ gap [36], and thus soft bases inhibitors are the most effective for metals. So, the APP I compound which has the lowest energy gap (ΔE) and the highest softness has the most inhibition efficiency.

To judge the adsorption centres in an inhibitor molecule for the interaction with metal surface Mulliken charge and dipole moment (μ) were also calculated. Mulliken population

analysis, establish the more negatively charged heteroatom that are the reactive sites [36] and labelled as N6, N7, N8, N11, N18, and O25 in the ring of pyrazole pyridine derivatives and given in Table 4. For the dipole moment (μ), some authors are in favor of low values [37] of the dipole moment and other favors in high value [38, 39] on the basis of dipole–dipole interaction of molecules and metal surface. In the present case lower value of μ obtained for APP I indicate the stronger interaction to metallic surface in comparison to other APPs.

3.4 Scanning electron microscopy analysis

The SEM micrographs for copper in absence and presence of optimum concentration of APP I after immersion of 72 h in 0.5 M HCl are represented in Figure 10a-b, respectively. It appears that the specimen surface was highly deteriorated, with some pits and cracks under inhibitor free condition (Figure 10a). The corresponding EDX profile (Figure 11a) having no oxygen peak, which indicates the breakdown of the air formed oxide film, and free corrosion of bare copper occurs. On the other hand, it is clearly seen in figure 10b corrosive attack has been suppressed, successfully, in presence of 1.59 mmol/L, APP I. The less damage surface indicates creation of physical barrier of adsorbed inhibitors between the metal and corrosive environment. According to given EDX analysis (Figure 11b), there is also an extra nitrogen peak was present. Even though its intensity is very low, it is an evidence for the role of nitrogen atoms for binding to copper surface. These EDX results prove that the APPs are effective corrosion inhibitors for copper in HCl.

4. Conclusions

This study has revealed that APPs are good inhibitors for copper corrosion in 0.5 HCl solutions. The order of inhibition efficiency is APP I > APP II > APP III at optimum concentration and maximum inhibition efficiency for APP I is 92.3%. Polarization measurements show that APPs are cathodic type inhibitors and results indicate that inhibitors have a stronger influence on the oxygen reduction than on the Cu oxidation reaction. The

impedance response in low frequency range revealed the film formation and diffusion controlled process at the copper-solution interface. Additionally, SEM and EDX studies of the copper surface indicate that the corrosion reaction was inhibited by adsorption of the APPs on the corroding copper surface. A good correlation has been found between Quantum chemical approach and experimentally obtained inhibition efficiencies.

Acknowledgment

Sudheer, express his deep thanks to Department of Chemistry, Indian Institute of Technology (Banaras Hindu University), Varanasi, India for financial support under Teaching Assistantship scheme.

References

- [1] M. G. Fontana, Corrosion Engineering, Mc Graw-Hill International, New York, 1987.
- [2] M. M. El-Naggar, *Corros. Sci.*, 2000, **42**, 773.
- [3] H. Ma, S. Chen, B. Yin, S. Zhao and X. Liu, *Corros. Sci.*, 2003, **45**, 867.
- [4] E. M. Sherif, and S.-M. Park, *Electrochim. Acta.*, 2006, **51**, 6556.
- [5] E.-S. M. Sherif, R. M. Erasmus and J. D. Comins, *Corros. Sci.*, 2008, **50**, 3439.
- [6] K. F. Khaled, *Electrochim. Acta.*, 2009, **54**, 4345.
- [7] M. M. Antonijević, S. M. Milić and M. B. Petrović, *Corros. Sci.*, 2009, **51**, 1228
- [8] M. S. El-Deab, *Mater. Chem. Phys.*, 2011, **129**, 223.
- [9] H. Tian, W. Li, K. Cao and B. Hou, *Corros. Sci.*, 2013, **73**, 281.
- [10] P. Wang, D. Zhang, R. Qiu, Y. Wan and J. Wu, *Corros. Sci.*, 2014, **80**, 366.
- [11] K. Krishnaveni and J. Ravichandran, *J. Electroanal. Chem.*, 2014, **735**, 24.
- [12] A. Ehsani, M. G. Mahjani, R. Moshrefi, H. Mostaanzadeh, and J. S. Shayeh, *RSC Adv.*, 2014, **4**, 20031.

- [13] H. Ma, S. Chen, L. Niu, S. Zhao, S. Li, and D. Li, *J. Appl. Electrochem.*, 2002, **32**, 65.
- [14] T. M. Fong, and S. B. Heymsfield, *Int J Obes.*, 2009, **33**, 947.
- [15] A. Dandia, S. L. Gupta¹, P. Singh, and M. A. Quraishi, *Sustainable Chem. Eng.*, 2013, **1**, 1303.
- [16] D. K. Yadav, D. S. Chauhan, I. Ahamad, and M. A. Quraishi, *RSC Adv.*, 2013, **3**, 632.
- [17] A. Rahmati, *Tetrahedron Lett.*, 2010, **51**, 2967.
- [18] K. F. Khaled, *Corros. Sci.*, 2010, **52**, 3225.
- [19] R. Solmaz, E. Altunbaş Şahin, A. Döner, and G. Kardaş, *Corros. Sci.*, 2011, **53**, 3231.
- [20] E.-S. Sherif, *J Solid State Electrochem.*, 2012, **16**, 891.
- [21] D. K. Yadav, and M. A. Quraishi, *Ind. Eng. Chem. Res.*, 2012, **51**, 1496.
- [22] W. Deng, P. Lin, Q. Li, and G. Mo, *Corros. Sci.*, 2013, **74**, 44.
- [23] M. Finšgar, *Corros. Sci.*, 2013, **68**, 51.
- [24] F. Caprioli, A. Martinelli, V. Di Castro, and F. Decker, *J. Electroanal. Chem.*, 2013, **693**, 86.
- [25] M. Finšgar and D. K. Merl, *Corros. Sci.*, 2014, **80**, 82.
- [26] A. Yurt and G. Bereket, *Ind. Eng. Chem. Res.*, 2011, **50**, 8073.
- [27] Y.-C. Pan, Y. Wen, L.-Y. Xue, X.-Y. Guo and H.-F. Yang, *J. Phys. Chem. C*, 2012, **116**, 3532.
- [28] E.-S. Sherif, *J Solid State Electrochem.*, 2012, **16**, 891.
- [29] Sudheer, and M. A. Quraishi, *Corros. Sci.*, 2013, **70**, 161.
- [30] E.-S. M. Sherif, *J. Ind. Eng. Chem.*, 2013, **19**, 1884–1889.

- [31] P. Song, X.-Y. Guo, Y.-C. Pan, S. Shen, Y. Sun, and Y. Wen, et al., *Electrochim. Acta.*, 2013, **89**, 503.
- [32] A. Döner, A. O. Yüce and G. Kardaş, *Ind. Eng. Chem. Res.*, 2013, **52**, 9709.
- [33] S. Zor, M. Saracoglu, F. Kandemirli and T. Arslan, *Corrosion*, 2011, **67**, 125003.
- [34] S. Issaadi, T. Douadi and S. Chafaa, *Appl. Surf. Sci.*, 2014, **316**, 582
- [35] Gaussian 03, Revision C.02, M. J. Frisch, G. W. Trucks, H. B. Schlegel, G. E. Scuseria, M. A. Robb, J. R. Cheeseman, J. A. Montgomery, Jr., T. Vreven, K. N. Kudin, J. C. Burant, J. M. Millam, S. S. Iyengar, J. Tomasi, V. Barone, B. Mennucci, M. Cossi, G. Scalmani, N. Rega, G. A. Petersson, H. Nakatsuji, M. Hada, M. Ehara, K. Toyota, R. Fukuda, J. Hasegawa, M. Ishida, T. Nakajima, Y. Honda, O. Kitao, H. Nakai, M. Klene, X. Li, J. E. Knox, H. P. Hratchian, J. B. Cross, C. Adamo, J. Jaramillo, R. Gomperts, R. E. Stratmann, O. Yazyev, A. J. Austin, R. Cammi, C. Pomelli, J. W. Ochterski, P. Y. Ayala, K. Morokuma, G. A. Voth, P. Salvador, J. J. Dannenberg, V. G. Zakrzewski, S. Dapprich, A. D. Daniels, M. C. Strain, O. Farkas, D. K. Malick, A. D. Rabuck, K. Raghavachari, J. B. Foresman, J. V. Ortiz, Q. Cui, A. G. Baboul, S. Clifford, J. Cioslowski, B. B. Stefanov, G. Liu, A. Liashenko, P. Piskorz, I. Komaromi, R. L. Martin, D. J. Fox, T. Keith, M. A. Al-Laham, C. Y. Peng, A. Nanayakkara, M. Challacombe, P. M. W. Gill, B. Johnson, W. Chen, M. W. Wong, C. Gonzalez, and J. A. Pople, Gaussian, Inc., Wallingford CT, 2007.
- [36] G. Gece, *Corros. Sci.*, 2008, **50**, 2981.
- [37] M. Mahdavian, and S. Ashhari, *Electrochim. Acta*, 2010, **55**, 1720.
- [38] M. K. Awad, M. R. Mustafa, and M. M. Abo Elnga, *J. Mol. Struct. (THEOCHEM)*, 2010, **959**, 66.
- [39] V. S. Sastri, Corrosion Inhibition Mechanisms, in: Green Corrosion Inhibitors, John Wiley & Sons, Inc., 2011: pp. 167–211.

Figure captions:

Figure 1: Synthetic route of APP derivatives.

Figure 2: Nyquist plots for copper in 0.5 M HCl containing different concentrations of (a) APP I (b) APP II(c) APP III.

Figure 3: Equivalent circuit model used to fit the impedance spectra.

Figure 4: Simulated (solid curves) and experimentally (dotted curves) Nyquist plots in absence and presence of 1.59 mmol of APP I, APP II, APP III.

Figure 5: Phase-impedance plots for copper in 0.5 M HCl in absence and presence of different concentrations of (a) APP I (b) APP II (c) APP III.

Figure 6: Potentiodynamic polarization curves for copper in 0.5 M HCl containing different concentrations of (a) APP I (b) APP II (c) APP III.

Figure 7: Cyclic voltammograms for copper obtained in 0.5 M HCl (a) bare copper and (b) 1.59 mmol of APP I in solution.

Figure 8: Optimized molecular structures (a) APP I (b) APP II and (c) APP III.

Figure 9: Frontier molecular orbital density distribution of (a) APP I (b) APP II and (c) APP III.

Figure 10: SEM micrographs of copper surfaces: (a) uninhibited 0.5 M HCl, and (b) in the presence of APP I.

Figure 11: EDX spectra of copper specimens: (a) uninhibited 0.5 M HCl, and (b) in the presence of APP I.

Figures

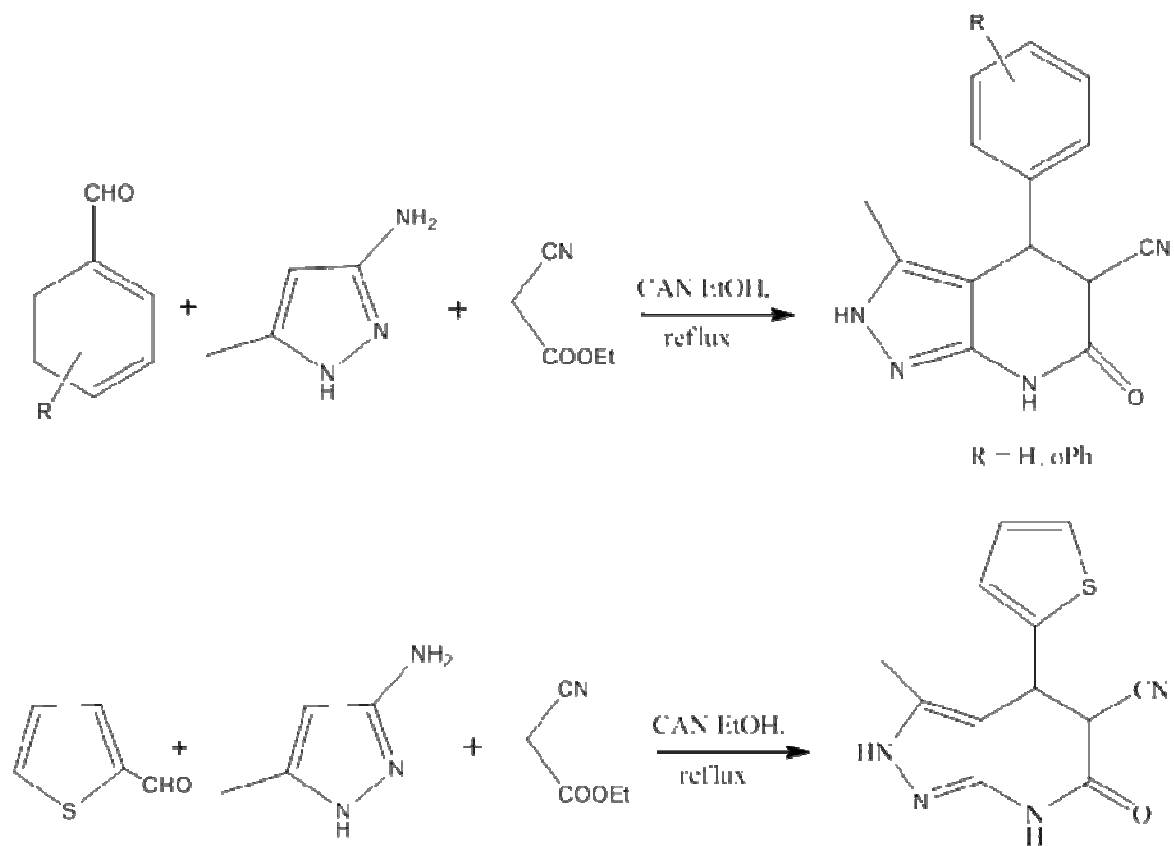
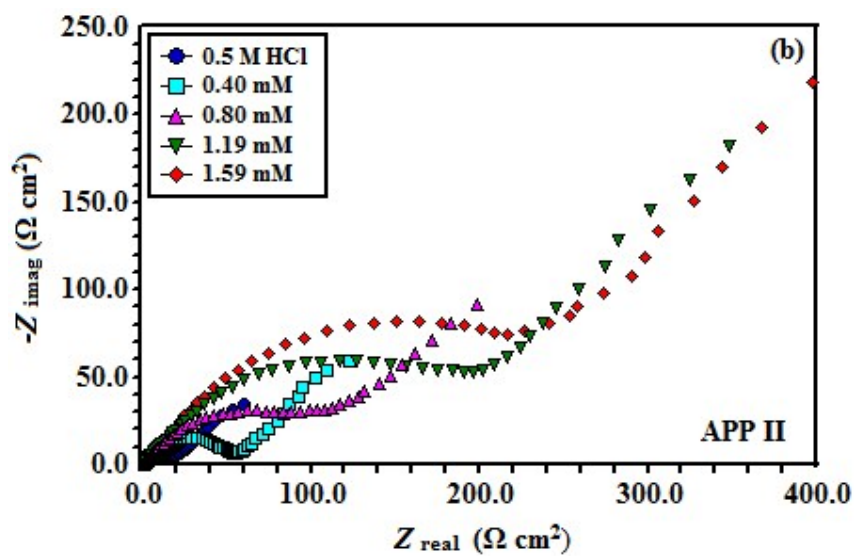
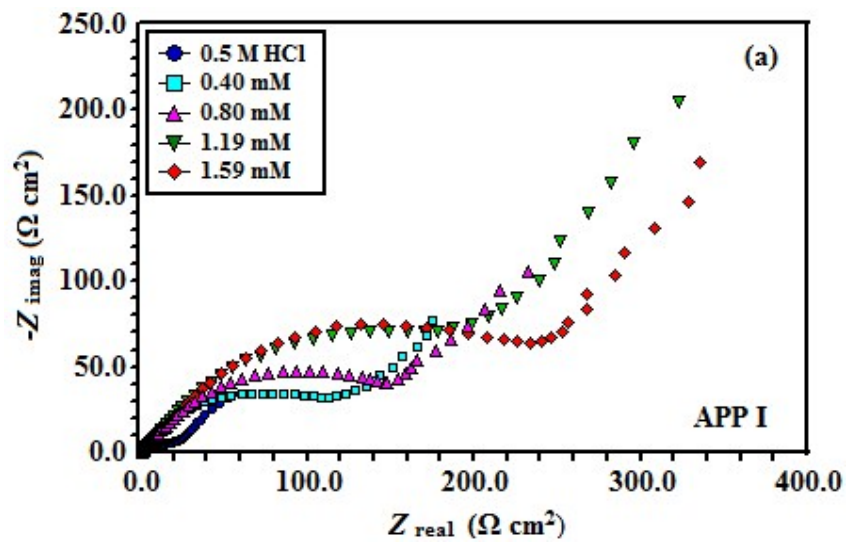


Figure 1. Synthetic route of APP derivatives



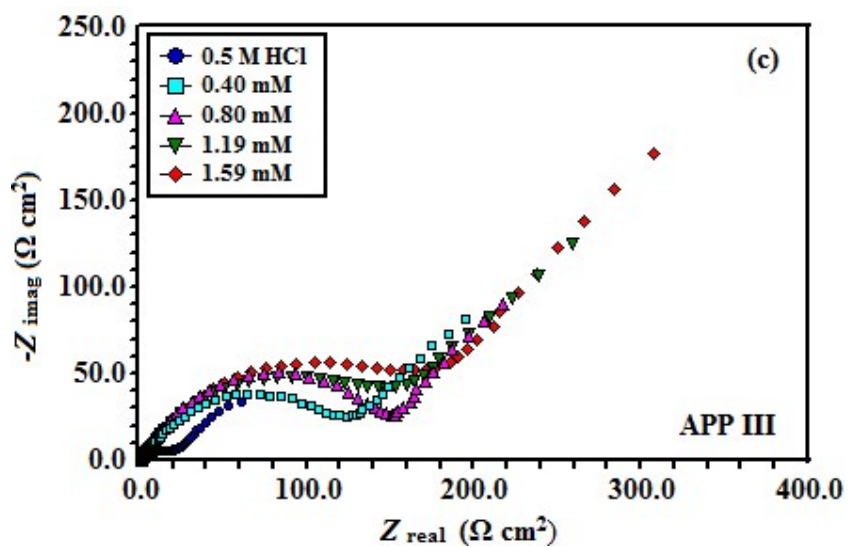


Figure 2: Nyquist plots for copper in 0.5 M HCl containing different concentrations of (a) APP I (b) APP II (c) APP III.

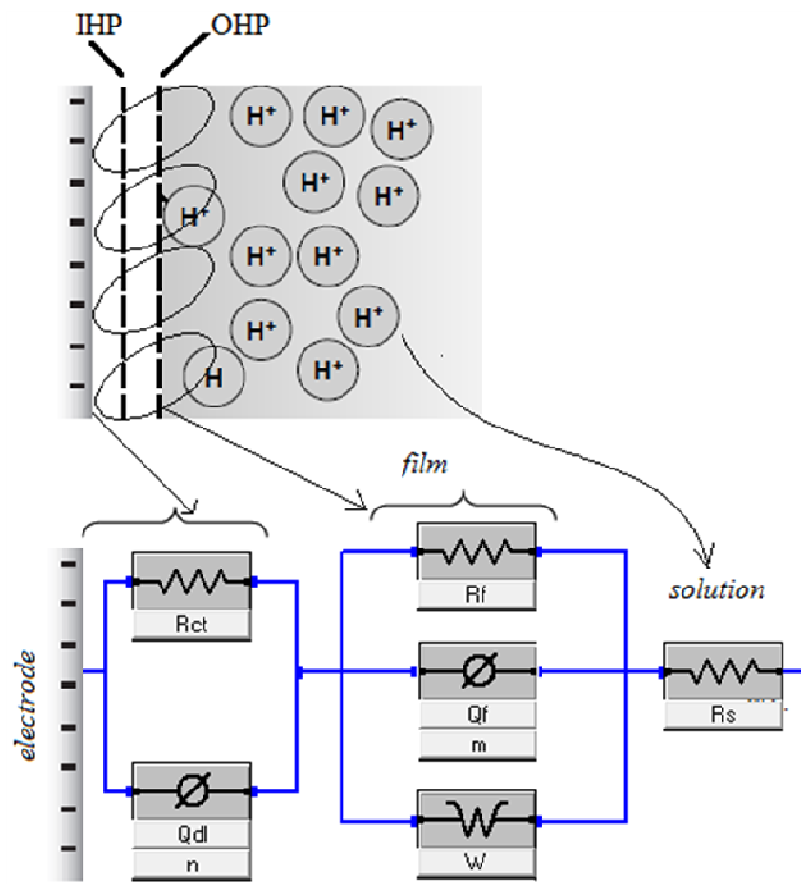


Figure 3: Equivalent circuit model used to fit the impedance spectra.

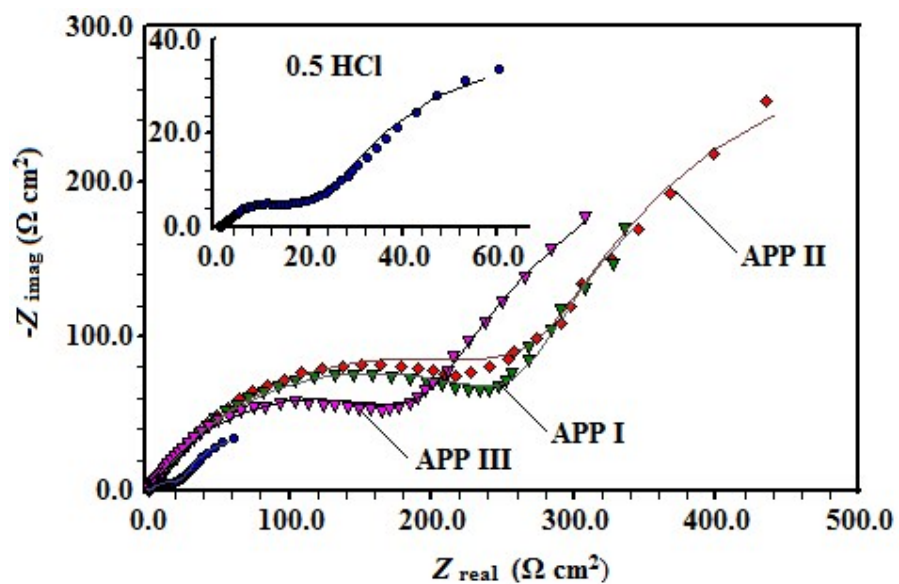
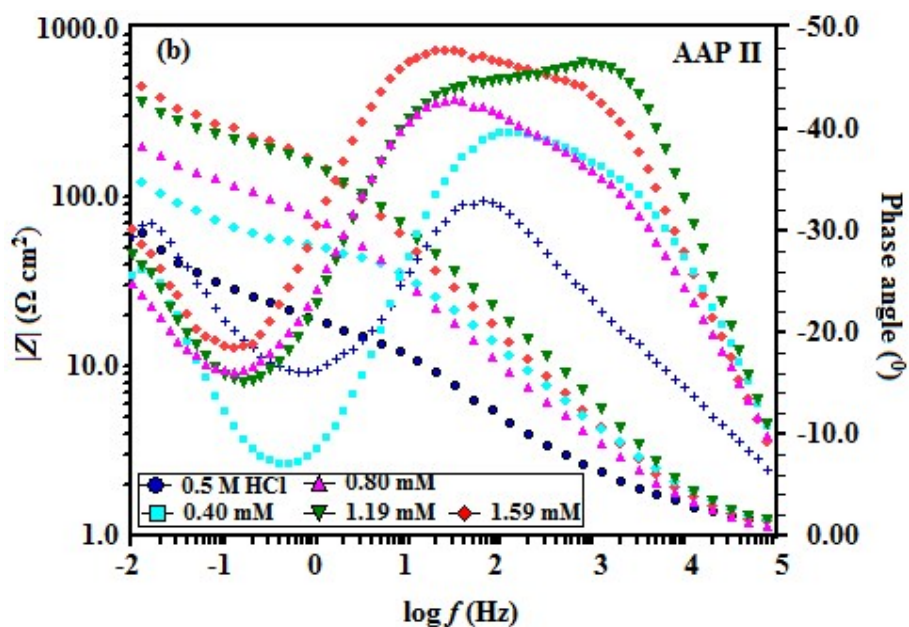
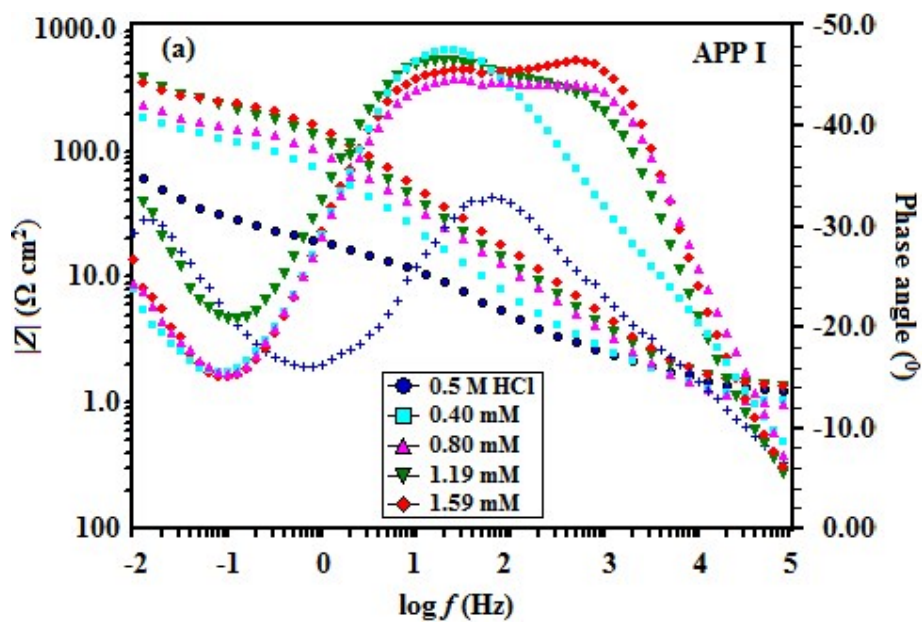


Figure 4: Simulated (solid curves) and experimentally (dotted curves) Nyquist plots in absence and presence of 1.59 mmol of APP I, APP II, APP III.



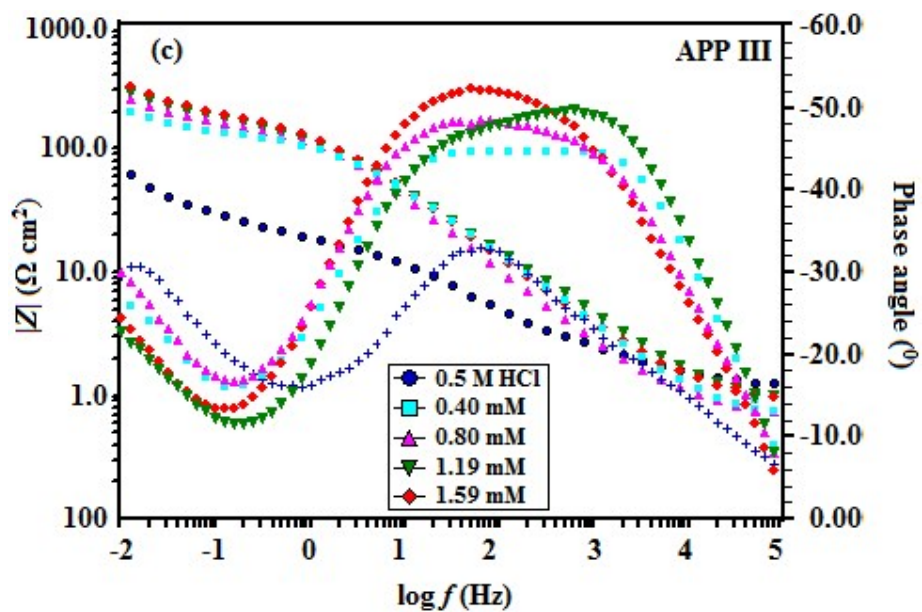
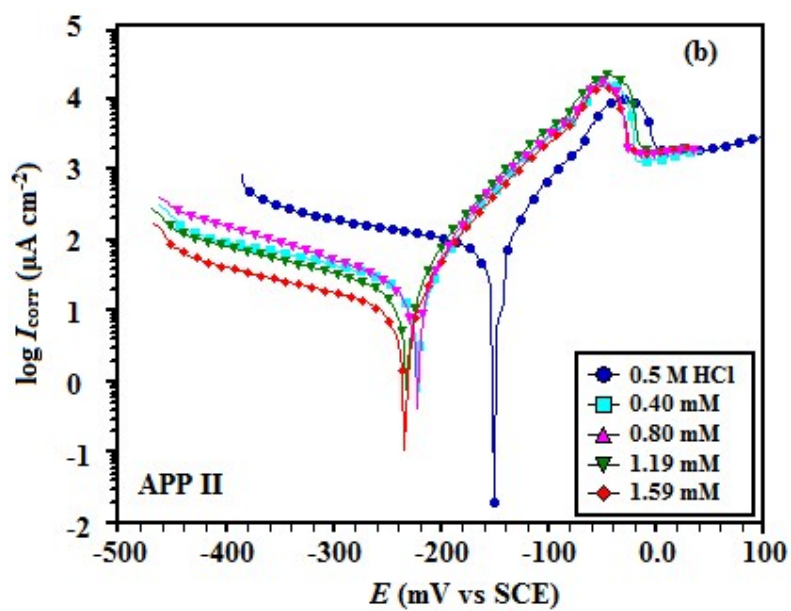
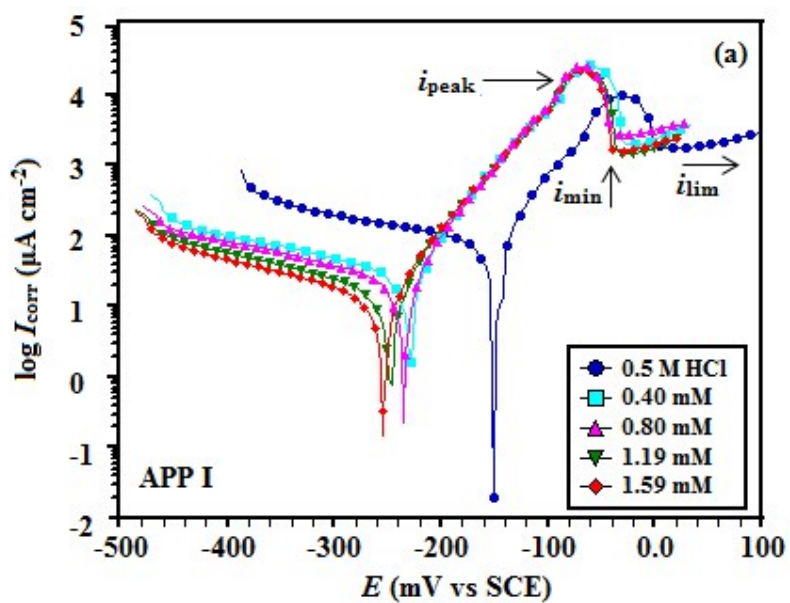


Figure 5: Phase-impedance plots for copper in 0.5 M HCl in absence and presence of different concentrations of (a) APP I (b) APP II (c) APP III.



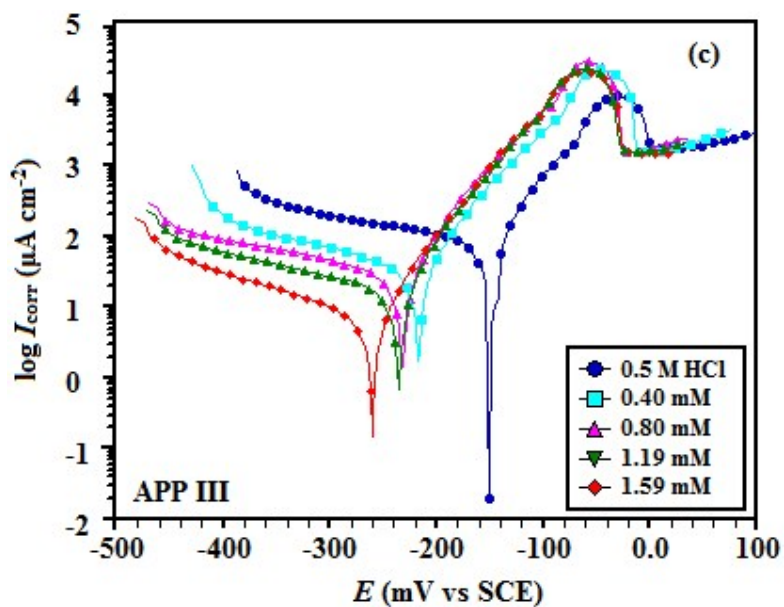


Figure 6: Potentiodynamic polarization curves for copper in 0.5 M HCl containing different concentrations of (a) APP I (b) APP II (c) APP III.

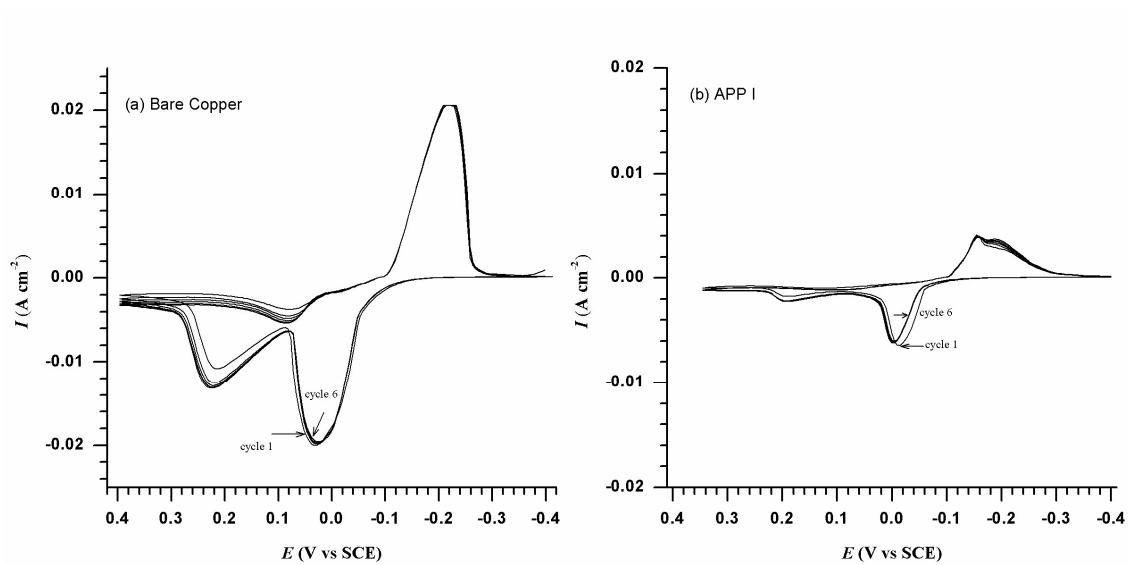


Figure 7: Cyclic voltammograms for copper obtained in 0.5 M HCl (a) bare copper and (b) 1.59 mmol of APP I in solution.

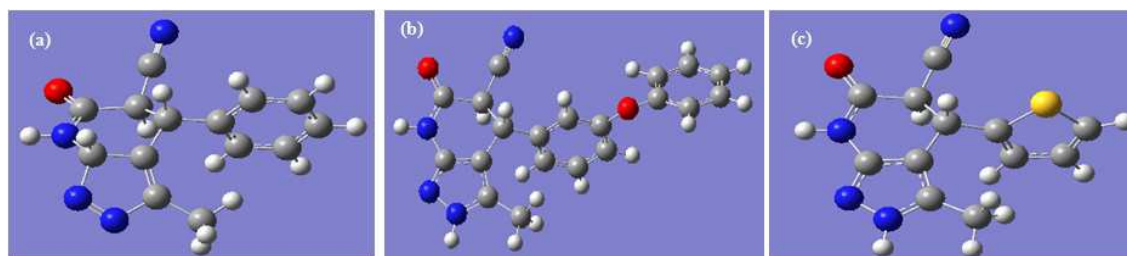


Figure 8: Optimized molecular structures (a) APP I (b) APP II and (c) APP III.

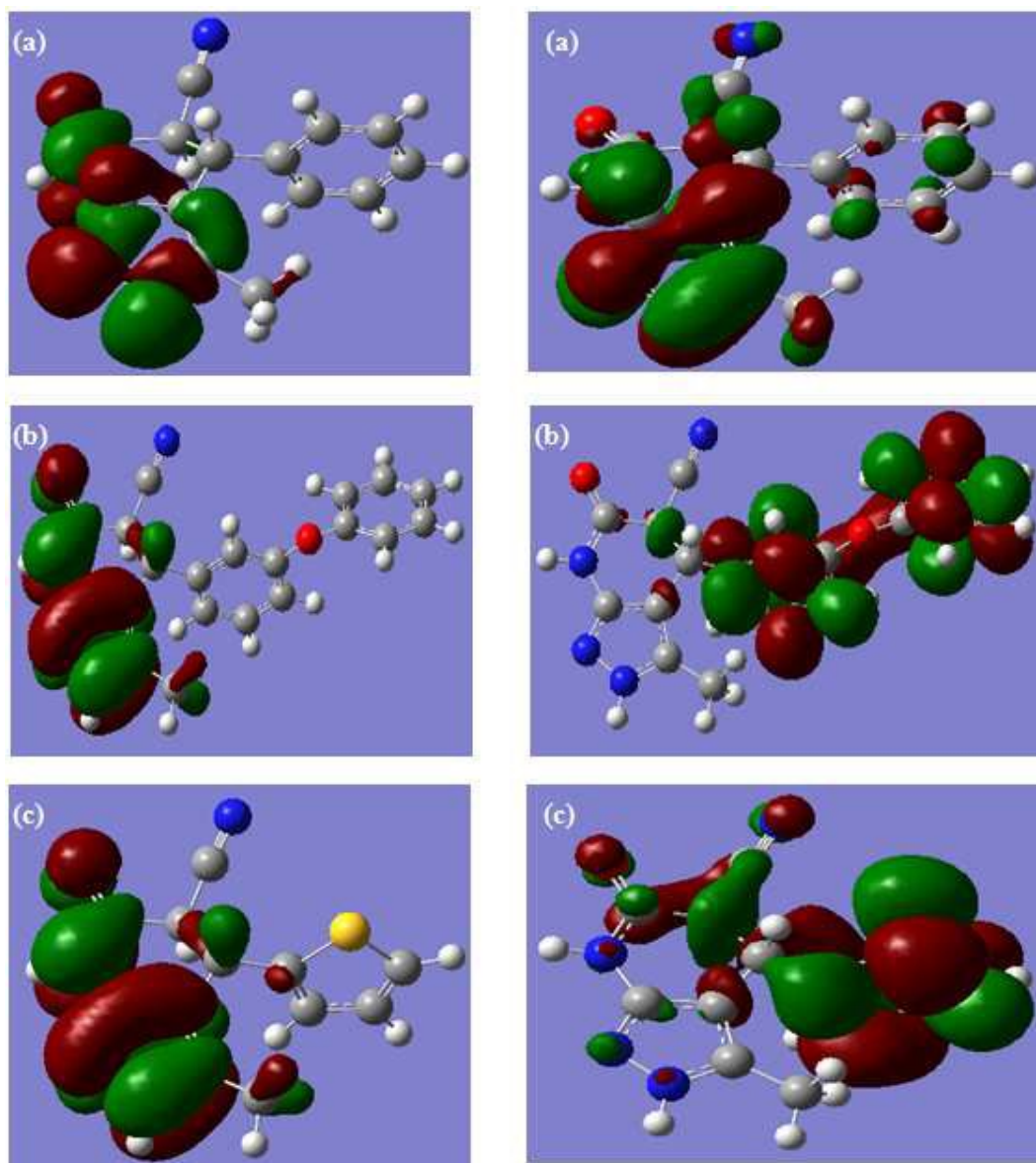


Figure 9: Frontier molecular orbital density distribution of (a) APP I (b) APP II and (c) APP III.

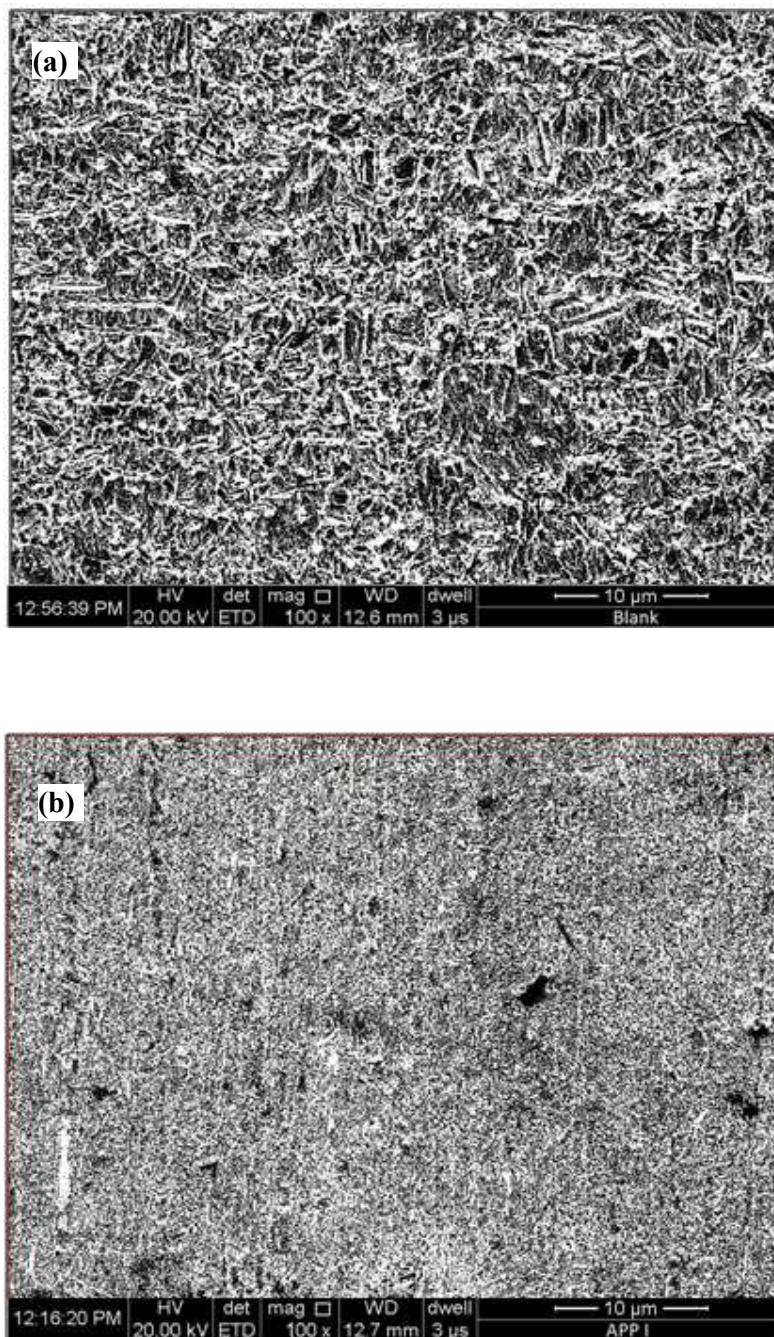


Figure 10: SEM micrographs of copper surfaces: (a) uninhibited 0.5 M HCl, and (b) in the presence of APP I

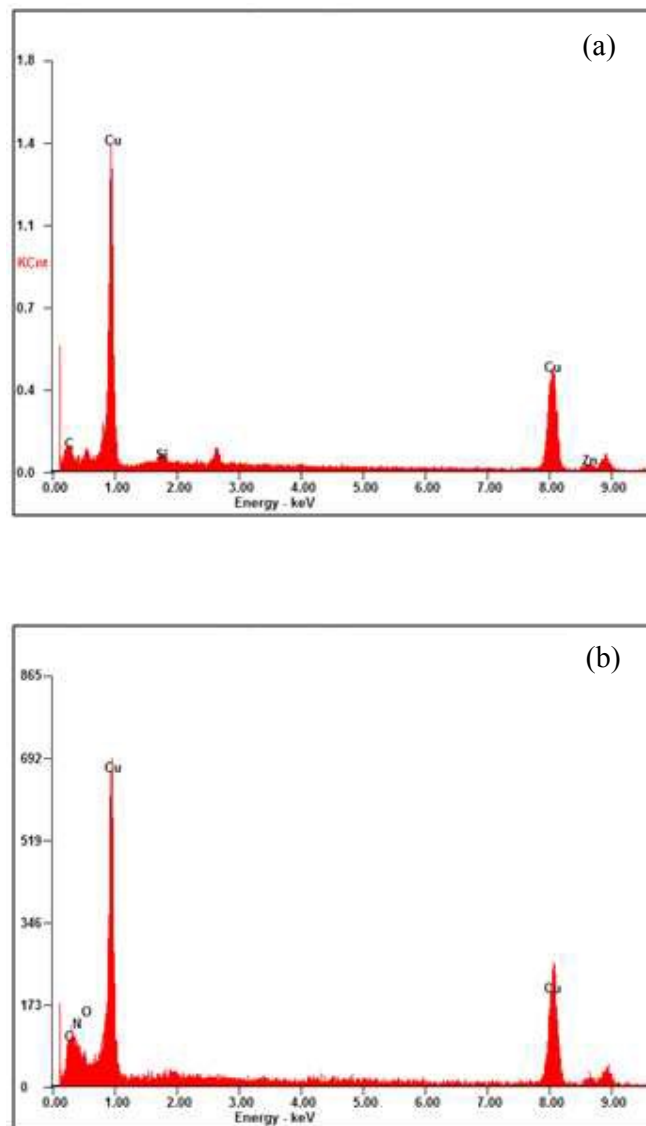


Figure 11: EDX spectra of copper surfaces: (a) uninhibited 0.5 M HCl, and (b) in the presence of APP I

Table 1: Molecular structure and analytical data for studied organic compounds as inhibitors.

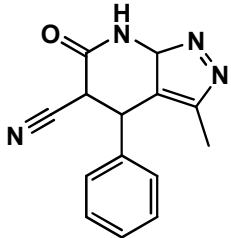
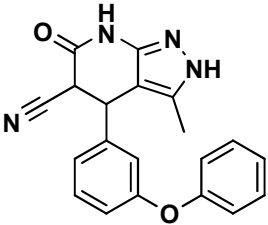
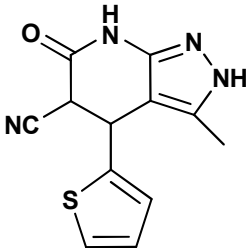
	<p>3-methyl-6-oxo-4,5,6,7-tetrahydro-2H-pyrazolo[3,4-<i>b</i>]pyridine-5-carbonitrile (APP I)</p>	<p>White powder; IR (KBr) cm^{-1}: 3570, 3290, 2240, 1710, 1535; ^1H NMR (300 MHz, $\text{DMSO-}d_6$) δ: 1.49 (s, 3H, CH_3), 4.41 (d, $^3J = 12.0$ Hz, 1H, CH), 4.65 (d, $^3J = 11.7$ Hz, 1H, CH), 7.12-7.56 (m, 5H, ArH), 10.96 (s, 1H, NH_{amid}), 11.99 (brs, 1H, $\text{NH}_{\text{pyrazole}}$) ppm. ^{13}C NMR (75 MHz, $\text{DMSO-}d_6$) δ: 9.95, 36.82, 43.92, 101.05, 117.58, 127.95, 128.66, 130.29, 135.77, 137.76, 147.68, 163.61 ppm.</p>
	<p>3-methyl-6-oxo-4-(3-phenoxyphenyl)-4,5,6,7-tetrahydro-2H-pyrazolo[3,4-<i>b</i>]pyridine-5-carbonitrile (APP II)</p>	<p>White powder; IR (KBr) cm^{-1}: 3568, 3284, 2238, 1705, 1542; ^1H NMR (300 MHz, $\text{DMSO-}d_6$) δ: 1.48 (s, 3H, CH_3), 4.50 (d, $^3J = 12.0$ Hz, 1H, CH), 4.69 (d, $^3J = 12.0$ Hz, 1H, CH), 7.14-7.63 (m, ArH, 9H), 10.96 (s, 1H, NH_{amid}), 12.00 (brs, 1H, $\text{NH}_{\text{pyrazole}}$) ppm. ^{13}C NMR (75 MHz, $\text{DMSO-}d_6$) δ: 9.92, 36.61, 43.98, 100.83, 115.91, 116.19, 116.77, 117.54, 129.77, 130.87, 135.69, 135.78, 136.61, 147.62, 160.48, 163.55 ppm.</p>
	<p>3-methyl-6-oxo-4-(thiophen-2-yl)-4,5,6,7-tetrahydro-2H-pyrazolo[3,4-<i>b</i>]pyridine-5-carbonitrile (APP III)</p>	<p>White crystalline solid; IR (KBr) cm^{-1}: 3570, 3282, 2248, 1716, 1534; ^1H NMR (300 MHz, $\text{DMSO-}d_6$) δ: 2.07 (s, 3H, CH_3), 4.38 (d, $^3J = 12.0$ Hz, 1H, CH), 4.64 (d, $^3J = 11.7$ Hz, 1H, CH), 6.97-7.51 (m, ArH, 3H), 10.99 (s, 1H, NH_{amid}), 12.10 (brs, 1H, $\text{NH}_{\text{pyrazole}}$) ppm. ^{13}C NMR (75 MHz, $\text{DMSO-}d_6$) δ: 10.01, 35.54, 42.39, 101.96, 117.07, 125.96, 126.21, 127.73, 135.07, 142.66, 146.84, 162.52 ppm.</p>

Table 2: Electrochemical impedance parameters accomplished by fitting the Nyquist plots with the equivalent circuit (Fig. 3) in absence and presence of various concentrations of APP I, APP II and APP III.

Conc. of inhibitor (mmol/L)	R_s (Ω cm^{-2})	Q_{dl}		R_{ct} (Ω cm^{-2})	Q_f		R_f ($\Omega \times 10^8$)	W ($\times 10^{-2}$)	$\eta\%$
		$Y_o \times 10^{-3}$	n		$Y_o \times 10^{-8}$	m			
		$(\Omega^{-1} \text{ s}^n \text{ cm}^{-2})$			$(\Omega^{-1} \text{ s}^n \text{ cm}^{-2})$				
Blank	1.14	8.25	0.58	17.9	0.069	0.44	0.000116	8.54	
APP I									
0.40	0.96	3.71	0.61	125.4	0.794	0.43	1.48	4.96	85.7
0.80	0.76	2.29	0.78	148.0	0.017	0.45	3.03	3.39	87.9
1.19	1.12	2.04	0.81	170.5	4.540	0.46	7.98	1.48	89.5
1.59	1.11	1.39	0.82	225.2	3.850	0.47	25.9	2.18	92.0
APP II									
0.40	1.03	1.79	0.59	52.7	0.821	0.44	0.56	5.23	65.9
0.80	0.94	3.20	0.74	114.5	0.482	0.45	1.41	3.80	84.3
1.19	0.89	1.15	0.79	183.4	0.164	0.45	4.33	1.79	90.2
1.59	0.98	1.49	0.83	220.2	0.175	0.46	6.08	1.38	91.8
APP III									
0.40	0.57	1.22	0.66	119.8	2.350	0.52	33.4	3.91	85.0
0.80	0.73	1.70	0.69	144.9	2.680	0.52	11.0	2.26	87.6
1.19	0.82	1.47	0.73	158.4	5.274	0.49	54.0	1.89	88.7
1.59	0.98	1.79	0.79	210.9	46.20	0.58	8.13	1.39	91.5

Table 3: Potentiodynamic polarization measurements parameters: in the absence and presence of various concentrations of APPs (I-III) for copper in 0.5 M HCl.

Inhibitor (mmol/L)	E_{corr} (mV vs.SCE)	$(E_{(H_2)})$ (mV vs.SCE)	$I_{E(H_2)}$ ($\mu\text{A cm}^{-2}$)	β_a (mV dec $^{-1}$)	β_c (mV dec $^{-1}$)	I_{corr} ($\mu\text{A cm}^{-2}$)	Inhibition efficiency
Blank	-149.0	-372.1	438.4	45.3	116.7	92.9	---
APP I							
0.40	-217.0	-400.4	202.8	50.5	239.8	41.1	55.9
0.80	-232.0	-441.4	128.8	52.5	307.7	32.4	65.1
1.19	-235.0	-443.0	095.1	44.7	243.9	16.3	82.5
1.59	-260.0	-457.6	071.9	50.3	218.8	7.1	92.3
APP II							
0.40	-222.0	-439.7	240.0	57.4	274.9	30.7	66.7
0.80	-223.0	-439.7	148.9	47.0	208.4	22.9	75.4
1.19	-237.0	-439.1	119.9	52.0	296.9	16.2	82.6
1.59	-234.0	-440.7	070.4	43.0	293.7	8.9	90.5
APP III							
0.40	-229.0	-446.9	157.7	51.4	280.8	32.4	65.1
0.80	-235.0	-453.3	127.9	53.7	247.9	26.0	72.0
1.19	-248.0	-462.4	110.1	50.7	262.6	15.9	82.8
1.59	-254.0	-463.5	096.8	55.6	301.3	12.9	86.1

Table 4: Quantum chemical parameters of APP I, APP II and APP III.

Inhibitors	E_{HOMO}	E_{LUMO}	ΔE	Mullikan charges					
				N_6	N_7	N_8	N_{11}	O_{18}	O_{25}
APP I	-6.9131	-2.3135	4.599	-0.5310	-0.2263	-0.1845	-0.4602	-0.4755	--
APP II	-6.1280	-0.6130	5.514	-0.6254	-0.3911	-0.3946	-0.4712	-0.5727	-0.4745
APP III	-6.3337	-0.7491	5.584	-0.6238	-0.3862	-0.3904	-0.4706	-0.4730	--